

Article

Experimental Investigation on the Motion Characteristics of Air-Floating Tripod Bucket Foundation during Free Floating

Xianqing Liu ^{1,*}, Yu Ding ¹, Wenlong Li ¹, Puyang Zhang ^{2,*}, Kui Yu ¹, Yutao Feng ¹, Nan Lv ³ and Sheng Luo ³

¹ National Engineering Research Center for Inland Waterway Regulation, Chongqing Jiaotong University, Chongqing 400074, China; 15023666772@163.com (Y.D.); lw1000614@163.com (W.L.); yukui_xk@126.com (K.Y.); ytaof@126.com (Y.F.)

² State Key Laboratory of Hydraulic Engineering Intelligent Construction and Operation, Tianjin University, Tianjin 300072, China

³ Department of Military Facilities, Army Logistics University of PLA, Chongqing 401331, China; 13696470884@163.com (N.L.); 13594168322@163.com (S.L.)

* Correspondence: liuxianqing_1986@126.com (X.L.); zpy@tju.edu.cn (P.Z.)

Abstract: In recent years, multi-bucket foundations have been studied and gradually adopted in engineering practices as a novel foundation for offshore wind turbines within a range of water depth of 30 to 50 m. This study investigated the motion characteristics of air-floating tripod bucket foundation (AFTBF) through a series of experiments during free air-floating. The experimental results show that the surge force appears to be the most important factor influencing pitch moment and motion, whether it is a change in water depth or a draft for AFTBF. The maximum amplitudes of surge acceleration and pitch angle show a trend of increasing with narrower spacing and decreasing with wider spacing, while the heave acceleration shows an opposite trend. The added mass and damping of heave motion for AFTBF increase with shallower water due to the increasing pressure difference between the inside and bottom of bucket foundation. The shallower the water depth and the larger the draft, the longer the resonance period of heave.

Keywords: tripod bucket foundation; air-floating; response amplitude operator (RAO); draft; water depth; spacing; heave; pitch



Citation: Liu, X.; Ding, Y.; Li, W.; Zhang, P.; Yu, K.; Feng, Y.; Lv, N.; Luo, S. Experimental Investigation on the Motion Characteristics of Air-Floating Tripod Bucket Foundation during Free Floating. *J. Mar. Sci. Eng.* **2024**, *12*, 187. <https://doi.org/10.3390/jmse12010187>

Academic Editor: Spyros A. Mavrakos

Received: 24 December 2023

Revised: 14 January 2024

Accepted: 16 January 2024

Published: 19 January 2024



Copyright: © 2024 by the authors. Licensee MDPI, Basel, Switzerland. This article is an open access article distributed under the terms and conditions of the Creative Commons Attribution (CC BY) license (<https://creativecommons.org/licenses/by/4.0/>).

1. Introduction

Wind power is a well-established and promising source of renewable energy for large-scale development and commercial use. It offers numerous benefits, including low environmental impact, sustainability, and high output. As technology advances and costs decrease, the global offshore wind power market is experiencing rapid growth [1,2]. One innovative foundation design that is currently being widely used in wind power development is the bucket foundation. There are three main types of bucket foundations used in offshore wind turbine engineering: mono-bucket foundation [3–5], composite bucket foundation [6,7], and multi-bucket foundations [8–10]. One of the main construction technologies used for composite and multi-bucket foundations is their air-floating characteristics. This technology has three main applications. The first is to tow out the bucket foundation through dock or building place and through shallow water. The foundation is raised or lowered by the pressure change of an air-cushion inside the structure; this method was used as part of the first composited bucket foundation, which was towed out from the dock to the construction site in 2010 [11,12]. The second application is to improve efficiency and reduce the cost of installing offshore wind turbines. This is achieved through the integrated floating transport technique of the composite bucket foundation to complete the transportation and installation simultaneously [13]. The third application is to reduce the loads during offshore operations and mooring. By storing air inside the bucket, the lifting

load during lowering is reduced, and the pressure is evenly distributed at the opening bottom, reducing the mooring load [14].

The construction environment for bucket foundations is typically calm seas, with known loads from wind, current, and waves [15,16]. The first two types of loads are usually applied to the structure as quasi-static loads. However, the open bottom of the bucket foundation can lead to dynamic interaction with waves, resulting in sudden changes in structural stress and motion response [17–20]. This can potentially lead to serious safety incidents. The construction equipment used for bucket foundations is diverse and large due to the size of wind turbines. This equipment is anchored or piled around the foundation, causing significant interaction [21,22]. Additionally, the structure's force and motion response are influenced by factors such as compartment design, number of buckets, water depth, and draft. Therefore, it is crucial to study the interaction between waves and bucket foundations.

The presence of an air cushion within the bucket foundation is the key distinguishing factor when comparing it to conventional floating structures, such as ships or ocean platforms. This is due to two main factors. First, the bucket foundation has an open bottom, which results in different performance compared to traditional structures with sealed bottoms. In traditional structures, the bottom acts as a rigid structure, interacting with the water spring. However, in the bucket foundation, the structure acts as a rigid structure on the series spring of both the air and water springs. Second, the compressed air within the bucket foundation has a significant impact on the force and motion characteristics of the structure. The lower stiffness of the gas and water springs in series, compared to the stiffness of the water spring alone, results in greater motion of the bucket foundation under the same force [23]. Additionally, the compressibility of the air cushion causes an increase in the volume of fluid entering and exiting the bucket foundation, leading to higher hydrodynamic parameters and a relatively slower movement of the structure [24].

Qi [25] studied the motion and mooring force of semi-submersible platforms and air-floating platforms, demonstrating that the air-floating supported structure has excellent motion performance and reduced mooring force. Kessel et al. [26] validated that very large floating structures (VLFS) supported by air cushions can significantly reduce bending moments. However, the advantages of air cushions for VLFS decline with an increase in the number of air cushions. Cheung et al. [27] derived the air-pocket factor by combining the ideal gas law and investigated the oscillation of the water column and the dynamic characteristics of a platform composed of an array of open-bottom cylinders. The forces in heave and pitch directions decrease with decreasing air-pocket factors. Bie et al. [28] presented the air buoyancy decrease coefficient to consider the impact on the stability and dynamic performance of air-floating structures. Thiagarajan et al. [29] presented a correction formula for the metacentric height, considering the net effect of the air cushion on the static stability of a compartmented air-floating structure.

Iwata et al. [30] conducted a study on the wave motions of a structure that was partially supported by an air cushion, using two-dimensional numerical analysis and model tests. The air pressure in the cushion was calculated using a linearized adiabatic law. The results showed that when the width-to-wavelength ratio was between 0.78 and 1.74, the heave motion observed in the tests was greater than that predicted by the numerical calculations. This was due to the simplification of the air state and the absence of attenuating waves. Pinkster et al. [31,32] modified the existing three-dimensional diffraction code DELFRAC to investigate the forces and motions of structures with one or more air cushions based on the adiabatic equation of an ideal gas. Malenica and Zalar et al. [33,34] proposed a method for solving the linear hydrodynamic problem of air-cushion supported structures. Compared to Pinkster's method, their approach included both kinematic and dynamic boundary conditions in the boundary value problems for the potentials. They then developed a semi-analytical solution for the heave motion of an air-floating cylinder using the method of matched asymptotic expansions. This solution was a significant achievement in solving special boundary value problems with a pressurized air-water

interface at the bottom. Lee and Newman [35] expanded the motion in the air compartment using an eigenfunction expansion. The interface elevation was described by a set of Fourier generalized modes with unknown amplitudes. The response of a very large floating structure (VLFS) with one cushion was investigated using the HIPAN problem. The results showed that the resonances in heave and pitch were caused by the interaction between body inertia, hydrostatic restoring, and the stiffness related to the volume change in the air compartment. Lee et al. [36] then extended this work to study the coupled motion characteristics of waves and air-floating structures. Zhang [37] derived the aerodynamic coefficients for heave motion for different types of air-cushion supported structures and studied the heave dynamic response of a floating wind turbine platform supported by an air cushion. The results showed that the natural period of heave motion increased with increasing water depth in shallow water but had little impact on heave performance in deep water.

Le et al. [38] analyzed the towing behaviors of a multi-bucket foundations platform through model tests and MOSES. It was found that shallow water has a significant impact on towing performance. Wang et al. [19] introduced an integral wet-towing method based on a wide shallow bucket jacket foundation and investigated the factors that affect stability and dynamic response. It was recommended to use this method for long-distance towing under level 5 wind and waves conditions. Zhang et al. [39] presented two lowering methods for multi-bucket jacket foundations. The initial air storage in the bucket can be between 5% and 15% and can be used to reduce the lifting loads and keep the stability of multi-bucket foundation during lowering. Yan et al. [40] proposed a new integrated wet-towing method for far-offshore applications, which involves a composite structure of "Jacket + Triple-bucket foundation". It was observed that the natural period of this structure increases with the draft, and when the wave period is close to the natural period, the foundation experiences a large dynamic response. Liu and Zhang et al. [41] established equations for the oscillating motion of an AFMBF and conducted model tests with varying drafts and spacing between buckets in shallow water.

The studies mentioned above focused on the stability and motion characteristics of various structures, including box-type air-floating structures with different compartments, single bucket foundations with multiple subdivisions, and multi-bucket foundations. On the one hand, previous studies have been conducted on the motion responses of multi-bucket foundations in shallow water [41]. However, these studies were limited by the use of elastic ropes to restrict the in-plane motion of the structure during testing. On the other hand, the forces exerted on multi-bucket foundations during the lowering process are typically the greatest at all stages. This is due to the presence of an air cushion inside the bucket, which can cause significant buoyancy and lead to tilting of the structure and relaxation of the suspension cable. This poses a serious safety risk during construction [24]. Therefore, the movement and response of multi-bucket foundations in an unconstrained state have a significant impact on the safe construction of a structure. These limitations could hinder the application of multi-bucket foundations in deeper water, where free floating is necessary. Therefore, it is important to study the oscillating motion characteristics of multi-bucket foundations in deep water.

Model testing is an effective method for observing experimental phenomena and evaluating the behavior of a model by changing specific control variables while keeping the environment and parameters constant. The rest of the paper is organized as follows: Section 2 provides details on the basic conditions and test combinations of the physical model test; Section 3 analyzes the response amplitude operators for surge, heave, and pitch in detail; and Section 4 summarizes the conclusions of this study.

2. Experimental Design

2.1. Model Parameters

The experiments, using scaled models, were conducted to study the motion responses of AFTBF during free floating. The wave period range of the prototype was 5–15 s, based

on real ocean conditions [42,43]. The water depth varied from 20 m to 40 m, covering both shallow and deep-water conditions. According to the calculation formula for wavelength in finite water depth, the wavelength range was determined to be 38–262 m. To account for the diffraction effect between the waves and the structure, as well as the hydrodynamic interaction between the buckets, a single bucket foundation with a diameter of 20 m ($D = 20$ m) was chosen. The spacing between the centers of the bucket top surfaces was 30 m, 40 m, and 50 m for Prototype 1, Prototype 2, and Prototype 3, respectively [44]. In the development of wind power, the main types of composite bucket foundations and multi-bucket foundations are wide and shallow buckets, so the height of each bucket was chosen as 10 m [45]. The similarity ratio between the prototype and the model, based on geometric and Froude similarity, was 1:100. The models were all made of stainless steel with a wall thickness of 1.0 mm. To avoid measurement errors caused by elastic deformation due to force and motion in waves, the two adjacent buckets were rigidly connected by plate connectors. The multi-bucket foundations were arranged in an equilateral triangle shape, and the detailed dimensions of the AFTBF prototypes are shown in Figures 1–3. It can be observed that the lengths of the plate connectors (S) for Prototype 1, Prototype 2, and Prototype 3 are 10 m, 20 m, and 30 m, respectively. Correspondingly, the lengths of S for Model 1, Model 2, and Model 3 are 0.1 m, 0.2 m, and 0.3 m, respectively. As shown in Figure 4, the origin (O) for the global coordinate system is located at the center of each structure’s top surface, and the detailed structural parameters for the models and prototypes are listed in Tables 1 and 2, respectively. M_b , M_g , and M_c are the mass of the bucket walls, bucket lids, and plate connectors for each structure, respectively.

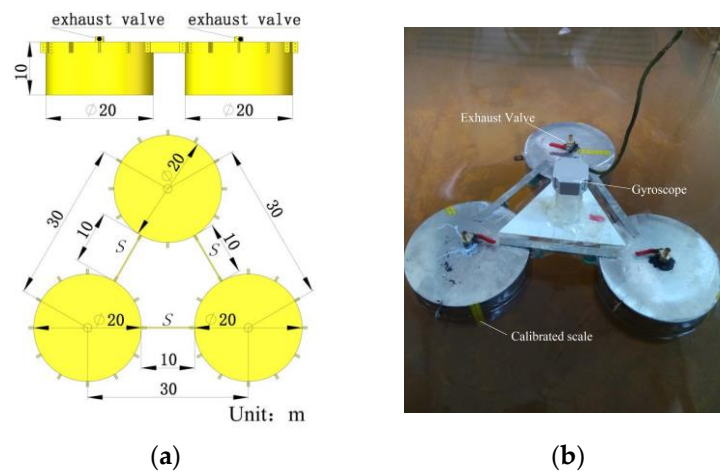


Figure 1. Prototype 1 and Model 1 of AFTBF with 0.5 D spacing: (a) Prototype 1; (b) Model 1.

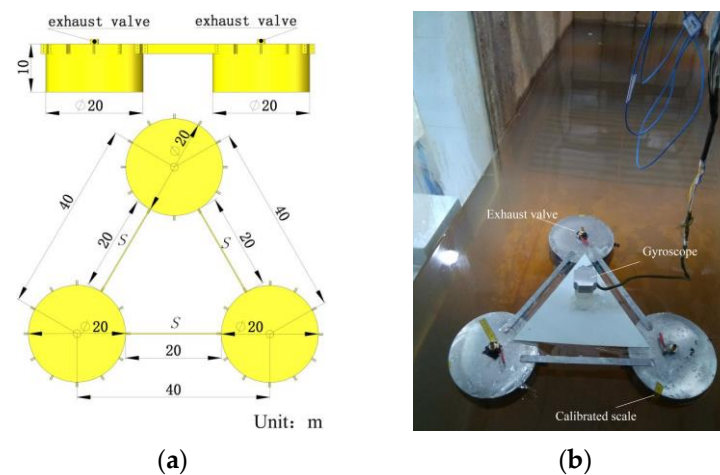


Figure 2. Prototype 2 and Model 2 of AFTBF with 1.0 D spacing: (a) Prototype 1; (b) Model 2.

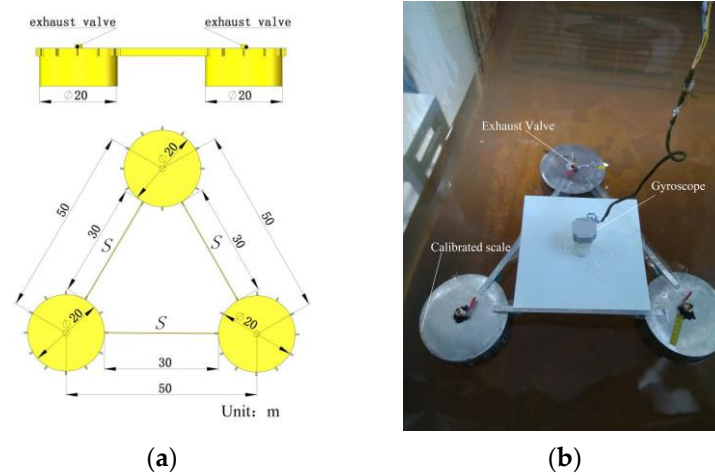


Figure 3. Prototype 3 and Model 3 of AFTBF with 1.5 D spacing: (a) Prototype 3; (b) Model 3.

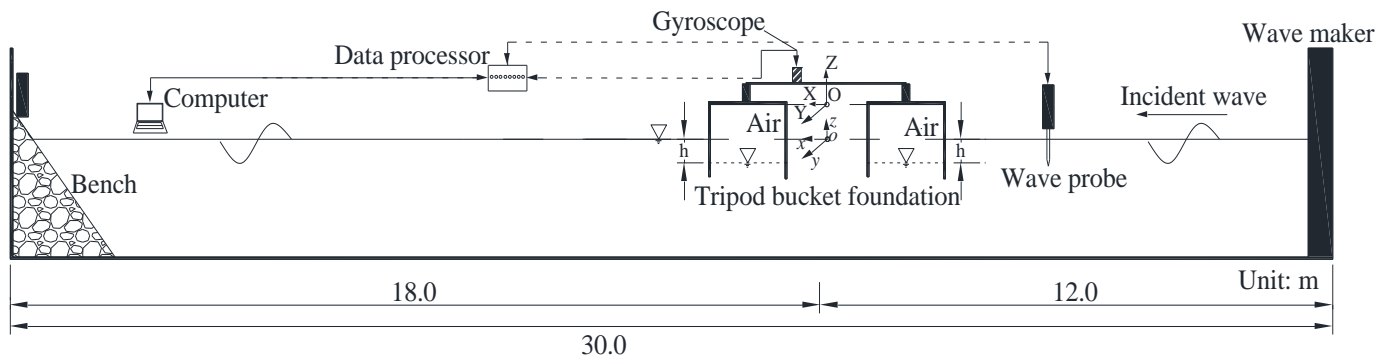


Figure 4. Schematic of the experimental setup.

Table 1. Main parameters of models.

Items	D (m)	H (m)	S (m)	M_b (kg)	M_g (kg)	M_c (kg)	Moment of Inertia (kg·m ²)		Gravity Center of Structure above O (m)
							J_x	J_y	
Model 1	0.2	0.1	0.1	1.665	0.738	0.047	3.23×10^{-2}	3.23×10^{-2}	(0.0, −0.0241)
Model 2	0.2	0.1	0.2	1.665	0.738	0.094	5.29×10^{-2}	5.29×10^{-2}	(0.0, −0.0237)
Model 3	0.2	0.1	0.3	1.665	0.738	0.143	8.09×10^{-2}	8.09×10^{-2}	(0.0, −0.0234)

Table 2. Main parameters of prototypes.

Items	D (m)	H (m)	S (m)	M_b (t)	M_g (t)	M_c (t)	Moment of Inertia (kg·m ²)		Gravity Center of Structure above O (m)
							J_x	J_y	
Prototype 1	20	10	10	1665	738	47.1	3.23×10^8	3.23×10^8	(0.0, −2.41)
Prototype 2	20	10	20	1665	738	94.2	5.29×10^8	5.29×10^8	(0.0, −2.37)
Prototype 3	20	10	30	1665	738	141.3	8.09×10^8	8.09×10^8	(0.0, −2.34)

2.2. Experiment Equipment and Arrangement

All tests were conducted in a wave flume located at the Key Laboratory of National Defense Engineering in Logistical Engineering University. The wave flume has dimensions of 30 m in length, 1.0 m in width, and 2.0 m in height. The hydraulic push plate wave maker was controlled by the control system to generate the required regular waves during the test. A YWH200-D wave probe, manufactured by Chengdu Xinda Shengtong Technology Co., Ltd. (Chengdu, China), was positioned at a predetermined distance from the wave maker to capture the time history of the wave height. The accuracy is $\pm 0.3\%$ of full range.

According to Section 6.2.5.4 of [46], the distance between the wave generator and the model in the test flume should be at least six times the average wavelength. For water depths of 20 m, 30 m, and 40 m, the corresponding average wavelengths are 1.18 m, 1.37 m, and 1.51 m, respectively, as shown in Table 3. Therefore, a distance of 12.0 m between the model and the wave generator would meet the requirements of the specification. At the top center position, a CS-VG-02A vertical gyroscope, produced by Xi'an Zhongxing Measurement and Control Co., Ltd. (Xi'an, China), was used to obtain the model's motion information. The accuracy of measured angle is less than 0.05°/s, while acceleration is less than 0.01 g. To ensure the accuracy and credibility of the tests, a wave dissipation device was installed at the end of the flume to eliminate any interference, such as reflected waves, on the measurement signal. A schematic of the experimental arrangement is shown in Figure 4. The origin (o) of the local Cartesian coordinate system for the structure is located at the model's center position on the surface of still water. The x-axis is parallel to the forward direction of wave propagation, the y-axis is perpendicular to the x-axis on the water surface, and the z-axis is perpendicular to the water surface.

Table 3. Experimental test conditions.

d (m)	Period (s)	L (m)	L/S		
			Model 1	Model 2	Model 3
0.20	0.5~1.5	0.38~1.98	1.52~7.92	1.27~6.60	1.09~5.66
0.30	0.5~1.5	0.39~2.35	1.56~9.40	1.30~7.83	1.11~6.71
0.40	0.5~1.5	0.39~2.62	1.56~10.48	1.30~8.73	1.11~7.49

2.3. Testing Procedures

It is widely recognized that the response amplitude operator (RAO) is a measure of the amplitude-frequency response of a structure when subjected to waves with specific periods and unit wave amplitude [47]. Therefore, all experimental combinations conducted in the flume focused on the interaction between regular waves and an aft buoyancy tank and were carried out under the conditions listed in Table 3. Based on the similarity criteria, the range of periods and water depths tested were 0.5–1.5 s and 0.2–0.4 m, respectively. The model's weight was supported by the pressure difference between the interior and exterior water surfaces of the buckets. Based on Equation (1) given in [15], the formula of weight balance is given below:

$$G = mg = (\rho \cdot g \cdot n \cdot h \cdot \pi \cdot D^2) / 4 \tag{1}$$

where G is the structure's weight, ρ is the density of water, g is the gravitational acceleration, n is the number of buckets, h is the required height of the pressure difference, and m is the sum of M_b, M_g, and M_c. Takes Model 1 as example:

$$G = mg = 2.45 \text{ kg} \times 9.82 \text{ m/s}^2 = 24.06 \text{ N}$$

$$h = G / (\rho \cdot g \cdot n \cdot h \cdot \pi \cdot D^2 / 4) \tag{2}$$

$$h = 24.06 / (9.82 \times 1025 \times 3 \times 3.14 \times 0.2^2 / 4) = 0.0254 \text{ m}$$

For Model 1, Model 2, and Model 3, the corresponding values of h were 0.0254 m, 0.0259 m, and 0.0263 m, respectively. To maintain stability and prevent air leakage, the chosen drafts for Models 1, 2, and 3 were 0.05 m, 0.06 m, and 0.07 m, respectively. The draft was adjusted by inflating or deflating the exhaust valve and using the calibrated scale attached to the bucket wall. According to Appendix B of [46], the time interval for collecting wave data in regular wave tests should be less than 1/20 of the average wave period. In this article, the minimum wave period is 0.5 s, and the required sampling interval is 0.025 s. To ensure the accuracy of the measurement signal, the sampling frequency of the gyroscope was set to 200 Hz in accordance with the operation and use guidelines to ensure the validity and accuracy of the data. The experimental data were processed using

Origin 2015 software, developed by OriginLab Company (Northampton, MA, USA) for data analysis, chart creation, and obtaining necessary information.

3. Results and Discussion

The gyroscope is capable of providing real-time acceleration signals in the translation direction, as well as angle and angular rate signals in the rotation direction of the structure. Based on the similarity criteria, the acceleration and angle of the model structure have a 1:1 similarity ratio with the prototype structure. This indicates that the motion of the prototype structure can be accurately described by the variation of the translational acceleration and rotational angle of the model structure [35]. To ensure the validity of the results, the maximum values of acceleration and angle at each cycle are averaged from the first three maximum amplitudes, as there are sufficient samples available. However, it should be noted that this study did not consider the influence of wave propagation direction on the structural motion response. During testing, the waves propagated along the length direction of the water tank, while the x-direction of the gyroscope was parallel to the wave propagation direction. As a result, this section will primarily focus on analyzing the characteristics of RAOs for the accelerations in heave and surge directions, as well as the angles in pitch direction, with varying water depths and drafts. All data and graphs are presented in model scale.

3.1. Validity of the Proposed Models

3.1.1. Validity 1

As shown in Table 1, during the model making process, the mass of the bucket wall, bucket cover, and connecting plates of each model were measured and weighed. Taking Model 1 as an example, if the density of stainless steel is 8000 kg/m^3 , the total mass of the bucket walls is:

$$M_b = n\pi DtH\rho = 3 \times 3.14 \times 0.2 \times 0.001 \times 0.1 \times 8000 = 1.507 \text{ kg} \quad (3)$$

The total mass of the bucket covers is:

$$M_g = n\pi D^2 t\rho/4 = 3 \times 3.14 \times 0.2^2 \times 0.001 \times 8000/4 = 0.754 \text{ kg} \quad (4)$$

The total mass of the connecting plates is:

$$M_c = nSBt\rho = 6 \times 0.1 \times 0.01 \times 0.001 \times 8000 = 0.048 \text{ kg} \quad (5)$$

The errors in the weighing and calculating masses of M_b , M_g , and M_c are 9.5%, 2.1%, and 2.1%, respectively, which are in good agreement.

3.1.2. Validity 2

From reference [41], it is evident that as the space (S) between the buckets increases, the pitch moment of inertia of the structure also increases. This trend is also reflected in the pitch angle of the structure, which decreases at the same water depth and draft. Figure 5 shows that the pitch angle RAO for various S values at a draft of 7.0 m and depths of 30 m and 40 m. It is apparent that as S increases, the pitch response of the structure decreases, indicating the effectiveness of the model test.

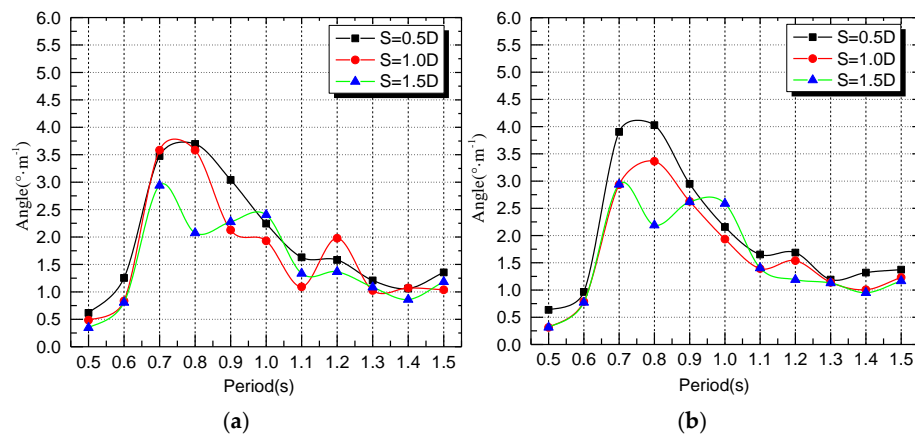


Figure 5. RAOs for Models with different S: (a) Water depth = 30 m; (b) Water depth = 40 m.

3.2. Effects of Depths

The RAOs of Model 1 in the surge, heave, and pitch directions at different water depths with a draft of 0.06 m are shown in Figure 6. The surge and heave acceleration, as well as pitch angle, all reach their maximum amplitude near the resonance period. When comparing Figure 6a,c, the trends between the surge and pitch directions are similar. The maximum amplitude increases with increasing water depth. However, the change in water depth from 30 m to 40 m is significantly greater than the change from 20 m to 30 m. This is due to the limited flow rate under the structure in shallower water, resulting in an increase in velocity and a decrease in pressure at the bottom of the structure. This leads to an increase in the draft of the structure, causing it to sink further. The added mass of surge motion and the added moment of inertia of pitch motion tend to increase, causing a decrease in surge acceleration and pitch angle in shallower water.

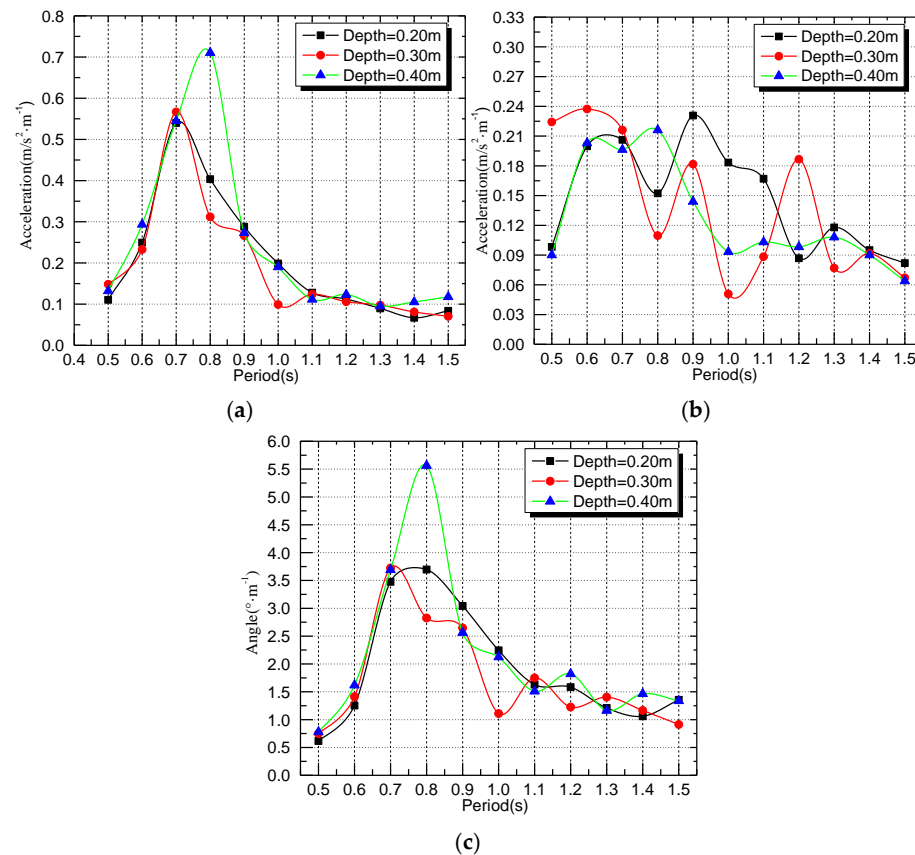


Figure 6. RAOs for Model 1 with different depths: (a) Surge; (b) Heave; (c) pitch.

Figure 6b shows three extreme values of heave acceleration within the measured period range. The period range and extreme values show a downward trend with increasing water depth. This can be attributed to two reasons. First, the incremental draft caused by the “shallow water effect” is reduced in deeper water. Second, the pressure difference between the inside and bottom of the bucket foundation increases, resulting in a greater amount of water entering and exiting the bottom of the structure. This increases the added mass of heave motion and reduces the heave acceleration. Additionally, the interaction between the buckets improves the oscillating characteristics of heave motion due to the narrower spacing of the buckets.

The RAOs of Model 2 in the surge, heave, and pitch directions at different water depths with a draft of 0.06 m are shown in Figure 7. Similar to Model 1, the surge and heave acceleration, as well as the pitch angle, all reach their maximum amplitudes near the resonance period. However, as the water depth increases, the maximum amplitudes of surge and heave acceleration, as well as pitch angle, first decrease and then increase. Additionally, the resonance periods for surge and pitch motion become longer, while the resonance period for heave motion becomes shorter. The reason is that the “shallow water effect” is weakened with wider spacing of the bucket and in deeper water. As a result, the pressure difference between the inside and bottom of the bucket foundation increases, leading to an increase in the stiffness of heave motion and a corresponding increase in the resonance frequency as the water depth increases.

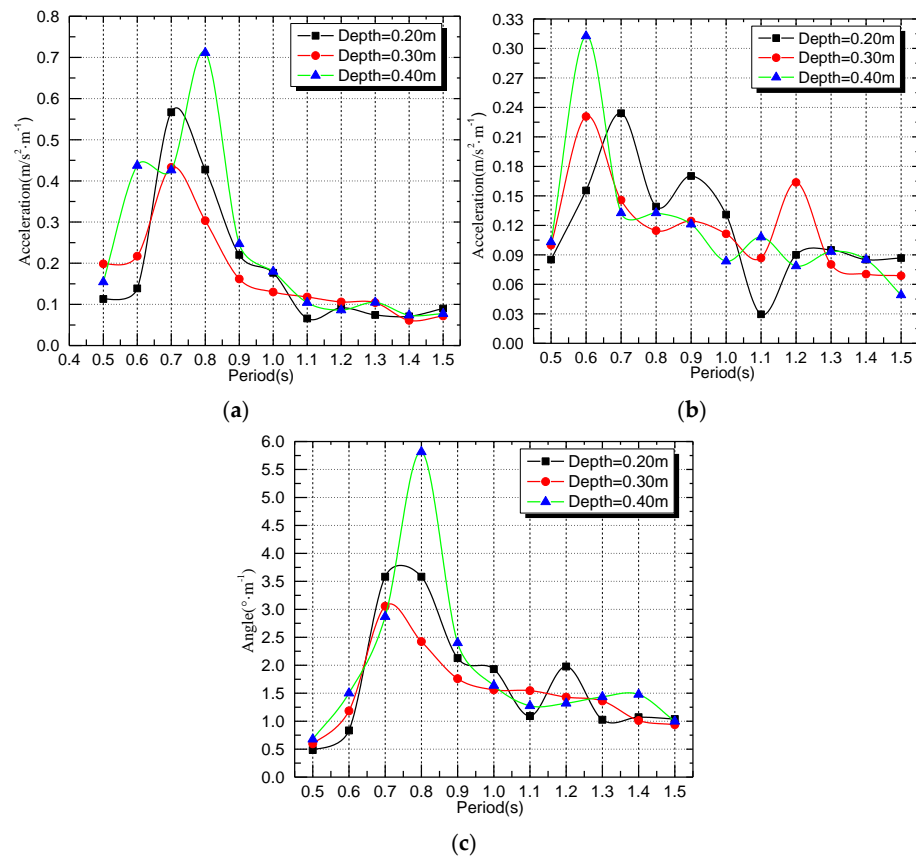


Figure 7. RAOs for Model 2 with different depths: (a) Surge; (b) Heave; (c) pitch.

The RAOs of Model 3 in the surge, heave, and pitch directions at different water depths with a draft of 0.06 m are shown in Figure 8. Similar to Models 1 and 2, the surge and heave acceleration, along with the pitch angle, reach their maximum amplitudes near the resonance period. The resonance period of heave motion becomes shorter with increasing water depth. However, despite the fact that the maximum amplitudes of surge and heave acceleration, as well as the pitch angle, decrease initially and then increase, the

maximum amplitude appears at a water depth of 20 m instead of 40 m. As is well known, the wider the spacing, the greater the moment of inertia of pitch motion. Additionally, it can be observed from Figures 5–7 that the “shallow water effect” is weakened and the hydrodynamic interaction between buckets decreases, resulting in a decrease in the response amplitude and oscillating characteristics of the structure’s motion with wider spacing. In other words, increasing the spacing between buckets improves the motion characteristics of the multi-bucket foundations.

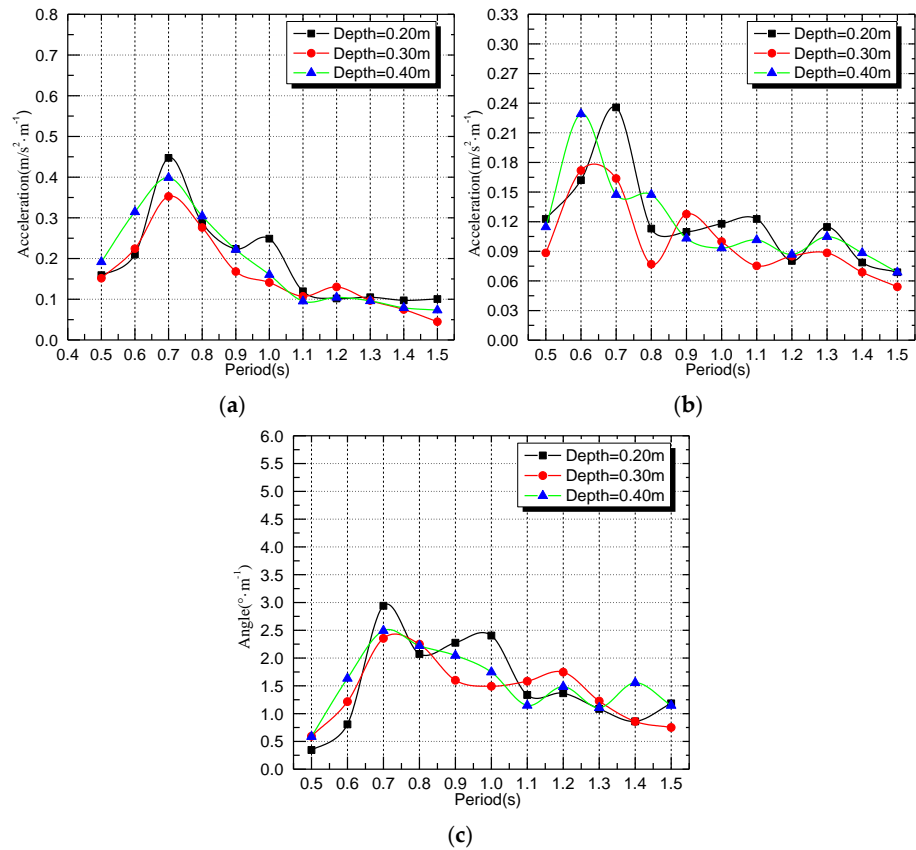


Figure 8. RAOs for Model 3 with different depths: (a) Surge; (b) Heave; (c) pitch.

3.3. Effects of Drafts

The RAOs of Model 1 in the surge, heave, and pitch directions at different drafts with a water depth of 0.2 m are shown in Figure 9. The maximum amplitudes of surge acceleration and pitch angle increase with an increase in draft. Additionally, the amplitude changes from a draft of 0.06 m to 0.07 m are greater than those from a draft of 0.05 m to 0.06 m. This is due to the increase in wave forces in the surge and pitch directions as the draft increases. However, the maximum amplitude of heave acceleration decreases as the added mass and damping of heave motion increase with a larger draft.

The RAOs of Model 2 in the surge, heave, and pitch directions at different drafts with a water depth of 0.2 m are shown in Figure 10. One notable difference between Model 1 and Model 2 is that the maximum amplitudes of surge and heave acceleration, as well as pitch angle, decrease with increasing draft. This can be attributed to the increase in added mass and added moment of inertia as the draft increases. Additionally, the hydrodynamic interaction between buckets is weakened and the wave force is decreased with larger spacings. As a result of the increased added mass and added moment of inertia in the heave and pitch directions, the resonance periods of heave and pitch motion also increase with larger drafts.

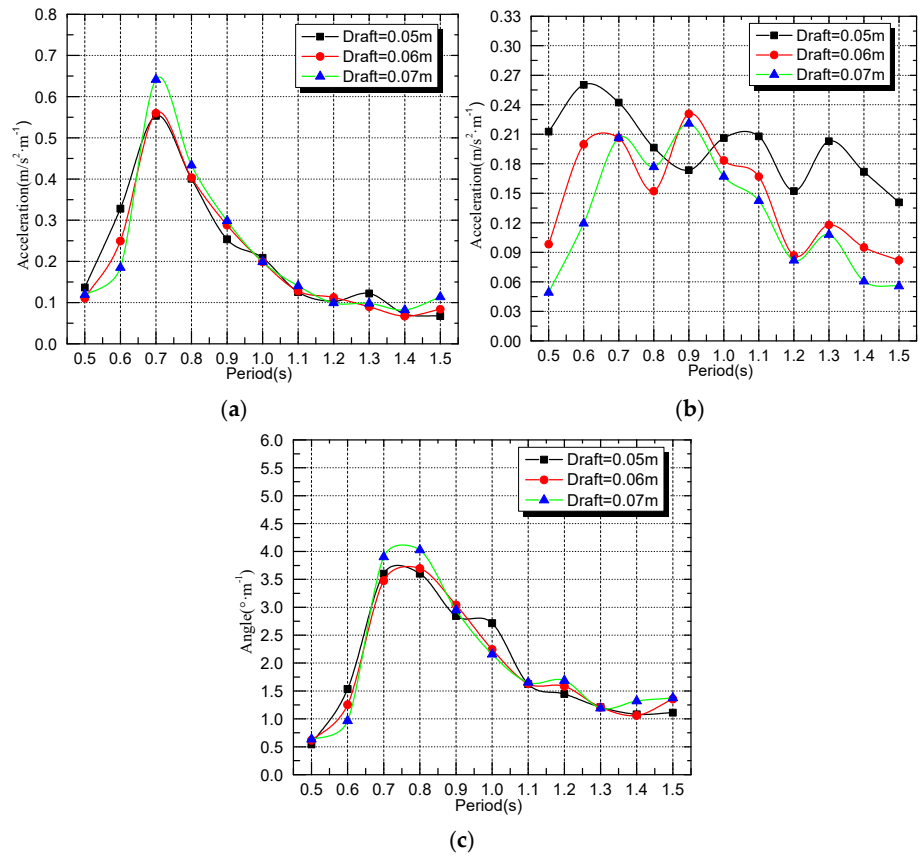


Figure 9. RAOs for Model 1 with different drafts: (a) Surge; (b) Heave; (c) pitch.

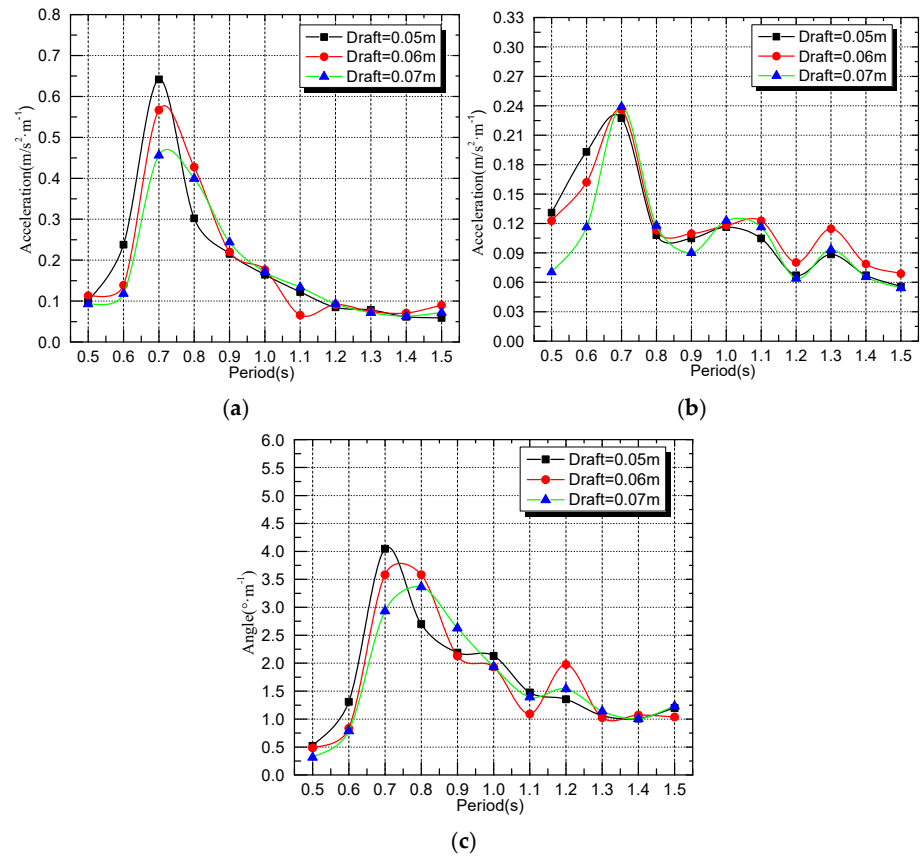


Figure 10. RAOs for Model 2 with different drafts: (a) Surge; (b) Heave; (c) pitch.

The RAOs of Model 3 in the surge, heave, and pitch directions at different drafts are shown in Figure 11. The resonance periods in the surge, heave, and pitch directions are all around 0.7 s. Similar to Model 2, as the draft increases, the maximum amplitudes of surge acceleration and pitch angle decrease. However, the maximum amplitude of heave acceleration increases slightly. Due to the fact that the primary masses involved in the heave motion are the structure’s mass and the water inside the buckets, the primary masses at drafts of 0.05 m, 0.06 m, and 0.07 m are 4.72 kg, 5.66 kg, and 6.61 kg, respectively. According to reference [41], the coefficient 1.2 can be considered the lower limit for a large draft, while 1.6 can be considered the upper limit for a small draft. For drafts of 0.05 m, 0.06 m, and 0.07 m, the added mass coefficients are 1.6, 1.4, and 1.2, respectively, resulting in masses involved in heave motion of 7.552 kg, 7.924 kg, and 7.932 kg. Figure 11a,c indicates that the pitch angle remains relatively constant at draft levels of 0.06 m and 0.07 m, while the surge motion shows a decreasing trend. This leads to a decrease in the mass of water entering and exiting the buckets, resulting in reduced damping and an increase in the heave acceleration of the structure. When compared to Model 1, Model 2, and Model 3, the trend of surge motion is consistent with pitch motion. The surge force appears to be the most important factor influencing pitch moment and motion. Additionally, as the spacing increases, the interaction between the buckets and the structure’s wave forces and hydrodynamic coefficients gradually decreases, resulting in a loss of oscillating motion response.

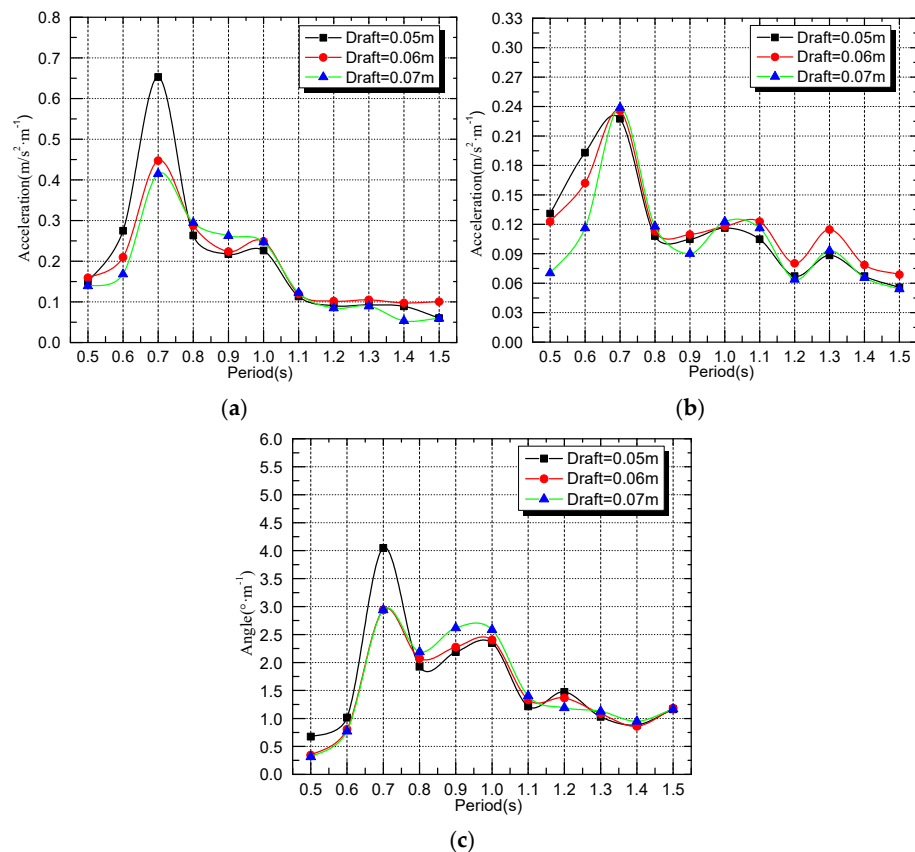


Figure 11. RAOs for Model 3 with different drafts: (a) Surge; (b) Heave; (c) pitch.

4. Conclusions

In this paper, physical model tests were conducted to investigate the motion responses characteristics of AFTBF, and the influence of different parameters on the RAOs in surge, heave and pitch directions was revealed. The main conclusions are as follows.

- (1) The results of wave tests with different water depths indicated that the maximum amplitudes of surge acceleration and pitch angle increase with narrower spacing while

first decrease and then increase with wider spacing. The oscillating characteristics of heave acceleration are weakened due to the hydrodynamic interaction between buckets in deeper water and with wider spacing.

- (2) The surge motion appears to be the most important factor influencing pitch motion, whether it is a change in water depth or a draft for AFTBF. The maximum amplitudes of surge acceleration and pitch angle show a trend of increasing with narrower spacing and decreasing with wider spacing, while the heave acceleration shows the opposite trend.
- (3) The added mass and damping of heave motion for AFTBF increase with shallower water due to the increasing pressure difference between the inside and bottom of the bucket foundation. The shallower the water depth and the larger the draft, the longer the resonance period of heave.

However, the interaction between waves and air-floating multi-bucket foundations has not been fully explored and developed in this research. Firstly, the similarity ratio was 1:100, but the scale effect on the RAOs was not investigated. Secondly, only the RAOs between regular waves with a common range of periods and the AFTBF were investigated, while those of irregular waves and AFTBF were not. Thirdly, only a constant D/H of 2 was considered in this study, while other D/H as well as d/H ratios were not investigated.

According to abovementioned limitations, further research should be carried out in the future: (1) the scale effect on the data correction should be studied, as the atmosphere is constant during tests; (2) the motion characteristics between irregular waves and air floating multi-bucket foundations should be investigated; (3) The effect of various D/H and d/H ratios on air floating multi-bucket foundation should be studied.

Author Contributions: Conceptualization, X.L., P.Z. and K.Y.; Methodology, X.L., P.Z. and K.Y.; Validation, W.L. and X.L.; Formal analysis, X.L. and Y.D.; Investigation, Y.F., P.Z. and X.L.; Resources: Y.D.; Data Curation, N.L. and S.L.; Writing-Original Draft Preparation, X.L., Y.D. and W.L.; Writing-Review and Editing, X.L., P.Z. and Y.D.; Supervision, P.Z. and Y.F.; Project Administration, P.Z., X.L. and K.Y.; Funding acquisition: P.Z., K.Y. and X.L. All authors have read and agreed to the published version of the manuscript.

Funding: This research was funded by the National Science Foundation of China (Grant No. 52171274), Science and Technology Research Program of Chongqing Municipal Education Commission (Grant No. KJQN202200740), China Railway Major Science and Technology Project (Grant No. 2022-Special-07-05 [06-03]), Team Building Project for Graduate Tutors in Chongqing (Grant No. 2022009), Research and Innovation Program for Graduate Students in Chongqing (Grant No. XM2022).

Institutional Review Board Statement: Not applicable.

Informed Consent Statement: Not applicable.

Data Availability Statement: Data are contained within the article.

Conflicts of Interest: The authors declare no conflicts of interest.

References

1. Wang, X.; Zeng, X.; Li, J.; Wang, H. A review on recent advancements of substructures for offshore wind turbines. *Energy Convers. Manag.* **2018**, *158*, 103–119. [[CrossRef](#)]
2. Wu, X.; Hu, Y.; Li, Y.; Yang, J.; Duan, L.; Wang, T.; Adcock, T.; Jiang, Z.; Gao, Z.; Lin, Z. Foundations of offshore wind turbines: A review. *Renew. Sustain. Energy Rev.* **2019**, *104*, 379–393. [[CrossRef](#)]
3. Byrne, B.; Houlsby, G.; Martin, C.; Fish, P. Suction caisson foundations for offshore wind turbines. *Wind Eng.* **2002**, *26*, 145–155. [[CrossRef](#)]
4. Zhao, X.; Chen, X.; Sui, S.; Deng, W.; Shen, K. Experimental study of local scour around bucket foundation in sand. *Ocean Eng.* **2023**, *286*, 115482. [[CrossRef](#)]
5. Zhang, C.; Wang, D.; Zheng, J. A cyclic-softening macro element model for mono-bucket foundations supporting offshore wind turbines in clay. *Comput. Geotech.* **2023**, *161*, 105603. [[CrossRef](#)]
6. Wang, L.; Zhang, J.; Cai, R.; Li, J. Wave effects on the anti-liquefaction of the seabed around composite bucket foundation of offshore wind turbines. *J. Hydrodyn.* **2022**, *33*, 1291–1302. [[CrossRef](#)]

7. Xiao, J.; Liu, J.; Lin, Y.; Zhang, P.; Gao, Y. Analysis of regular wave floating characteristics of mono-column composite bucket foundation during towing. *Energies* **2023**, *16*, 5076. [[CrossRef](#)]
8. Kim, D.; Choo, Y.; Kim, J.; Kim, S.; Kim, D. Investigation of monotonic and cyclic behavior of tripod suction bucket foundations for offshore wind towers using centrifuge modeling. *J. Geotech. Geoenviron.* **2014**, *140*, 04014008. [[CrossRef](#)]
9. Faizi, K.; Faramarzi, K.; Dirar, S.; Chapman, D. Investigating the monotonic behaviour of hybrid tripod suction bucket foundations for offshore wind towers in sand. *Appl. Ocean Res.* **2019**, *89*, 176–187. [[CrossRef](#)]
10. Barari, A.; Glittrup, K.; Christiansen, L.; Ibsen, L.; Choo, Y. Tripod suction caisson foundations for offshore wind energy and their monotonic and cyclic responses in silty sand: Numerical predictions for centrifuge model tests. *Soil Dyn. Earthq. Eng.* **2021**, *149*, 106813. [[CrossRef](#)]
11. Ding, H.; Feng, Z.; Zhang, P.; Le, C. Integrated towing transportation technique for offshore wind turbine with composite bucket foundation. *China Ocean Eng.* **2022**, *1*, 036. [[CrossRef](#)]
12. Song, H.; Yu, T.; Yu, D.; Zhao, Z. Hydrodynamic behaviour of composite bucket foundation with random waves. *Ocean Eng.* **2023**, *281*, 114774. [[CrossRef](#)]
13. Meng, L.; Ding, H. Experimental study on the contact Force between the vessel and CBF in the integrated floating transportation process of offshore wind power. *Energies* **2022**, *15*, 7970. [[CrossRef](#)]
14. Zhang, P.; Zhang, S.; Wei, Y.; Le, C.; Ding, H. Hydrodynamic characteristics of the crane vessel-three-bucket jacket foundation coupling hoisting system during the process of lowering. *Ocean Eng.* **2022**, *250*, 111034. [[CrossRef](#)]
15. Zhang, P.; Ding, H.; Le, C. Hydrodynamic motion of a large prestressed concrete bucket foundation for offshore wind turbines. *J. Renew. Sustain. Energy* **2013**, *5*, 063126. [[CrossRef](#)]
16. Zhang, P.; Qi, X.; Wei, Y.; Le, C.; Ding, H. Hydrodynamic characteristics of three-Bucket jacket foundation for offshore wind turbines during the lowering process. *China Ocean Eng.* **2023**, *37*, 73–84. [[CrossRef](#)]
17. Ikoma, T.; Rheem, C.; Masuda, K.; Maeda, H. Response reduction of motion and steady wave drifting forces of floating bodies supported by air-cushions in regular waves. In Proceedings of the 25th International Conference on Offshore Mechanics and Arctic Engineering, Hamburg, Germany, 4–9 June 2006.
18. He, F.; Huang, Z.; Law, A. Hydrodynamic performance of a rectangular floating breakwater with and without pneumatic chambers: An experimental study. *Ocean Eng.* **2012**, *51*, 16–27. [[CrossRef](#)]
19. Wang, H.; Liu, C.; Guo, Y.; Zhao, Y.; Li, X.; Lian, J. Experimental and numerical research on the wet-towing of wide-shallow bucket foundation for offshore substation. *Ocean Eng.* **2023**, *275*, 114126. [[CrossRef](#)]
20. Li, L.; Gao, Z.; Moan, T.; Ormberg, H. Analysis of lifting operation of a monopile for an offshore wind turbine considering vessel shielding effects. *Mar. Struct.* **2014**, *39*, 287–314. [[CrossRef](#)]
21. Li, L.; Gao, Z.; Moan, T. Response analysis of a nonstationary lowering operation for an offshore wind turbine monopile substructure. *J. Offshore Mech. Arct.* **2015**, *137*, 051902. [[CrossRef](#)]
22. Li, L.; Gao, Z.; Moan, T. Analysis of lifting operation of a monopile considering vessel shielding effects in short-crested waves. *Int. J. Offshore Polar* **2016**, *26*, 408–416. [[CrossRef](#)]
23. Dominique, R.; Christian, C.; Alexia, A.; Alla, W. Wind Float: A floating foundation for offshore wind turbines. *J. Renew. Sustain. Ener.* **2010**, *2*, 33104. [[CrossRef](#)]
24. Wei, Y. Dynamic Characteristics Analysis of Three Bucket Jacket for Offshore Wind Turbines during Lowering Process. Ph.D. Thesis, Tianjin University, Tianjin, China, 2020.
25. Qi, X. Experimental study on behavior of an open bottom floating platform in wave, wind and current. In Proceedings of the 4th International Offshore and Polar Engineering Conference, Osaka, Japan, 10–15 April 1994.
26. Van Kessel, J.; Pinkster, J. Wave-induced structural loads on different types of air-cushion supported structures. In Proceedings of the International Offshore and Polar Engineering Conference, Lisbon, Portugal, 1 July 2007.
27. Cheung, K.; Phadke, A.; Smith, D.; Lee, S.; Seidl, L. Hydrodynamic response of a pneumatic floating platform. *Ocean Eng.* **2000**, *27*, 1407–1440. [[CrossRef](#)]
28. Bie, S.; Ji, C.; Ren, Z.; Li, Z. Study on floating properties and stability of air floated structures. *China Ocean Eng.* **2002**, *16*, 263–272.
29. Thiagarajan, K. Hydrostatic stability of compartmented structures supported by air cushions. *J. Ship Res.* **2009**, *53*, 151–158. [[CrossRef](#)]
30. Iwata, K. Characteristics of Motion Response of a Floating Structure supported by Air cushion in Waves. *Proc. Coast. Eng.* **1986**, *33*, 531–535. (In Japanese)
31. Pinkster, J. The effect of air cushions under floating offshore structures. In Proceedings of the Behaviour of Offshore Structures (BOSS '97), Delft, The Netherlands, 7–10 July 1997.
32. Pinkster, J.; Fauzi, A.; Inoue, Y.; Tabeta, S. The behavior of large air cushion supported structures in waves. In Proceedings of the 2nd International Conference of Hydro-Elasticity in Marine Technology, Fukuoka, Japan, 1–3 December 1998.
33. Malenica, S.; Zalar, M. An alternative method for linear hydrodynamics of air cushion supported floating bodies. In Proceedings of the 15th International Workshop on Water Waves and Floating Bodies, Caesarea, Israel, 17 February–1 March 2000.
34. Malenica, S.; Zalar, M. Semi analytical solution for heave radiation of the air cushion supported vertical circle cylinder in water of finite depth. In Proceedings of the 16th International Workshop on Water Waves and Floating Bodies, Hiroshima, Japan, 22–25 April 2001.
35. Lee, C.; Newman, J. Wave effects on large floating structures with air cushions. *Mar. Struct.* **2000**, *13*, 315–330. [[CrossRef](#)]

36. Lee, C.; Newman, J. An extended boundary integral equation for structures with oscillatory free-surface pressure. *Int. J. Offshore Polar* **2016**, *26*, 41–47. [[CrossRef](#)]
37. Zhang, X. The Analysis of Diffraction and Heave Dynamic Performance for a Floating Wind Turbine Platform Supported by Aircushion. Ph.D. Thesis, Harbin Engineering University, Harbin, China, 2018.
38. Le, C.; Ding, H.; Zhang, P. Air floating towing behaviors of multi-bucket foundation platform. *China Ocean Eng.* **2013**, *27*, 645–658. [[CrossRef](#)]
39. Zhang, P.; Ren, J.; Li, Y.; Le, C.; Ding, H. Experimental research on the lowering process of the three and four-bucket jacket foundation of offshore wind turbine. *Ocean Eng.* **2023**, *286*, 115600. [[CrossRef](#)]
40. Yan, C.; Wang, H.; Guo, Y.; Wang, Z.; Liu, X. Laboratory study of integrated wet-towing of a triple-bucket jacket foundation for far-offshore applications. *J. Mar. Sci. Eng.* **2021**, *9*, 1152. [[CrossRef](#)]
41. Liu, X.; Zhang, P.; Zhao, M.; Ding, H.; Le, C. Air-floating characteristics of large-diameter multi-bucket foundation for offshore wind turbines. *Energies* **2019**, *12*, 4108. [[CrossRef](#)]
42. Lombardi, D.; Bhattacharya, S.; Muir, W.D. Dynamic soil structure interaction of monopile supported wind turbines in cohesive soil. *Soil Dyn. Earthq. Eng.* **2013**, *49*, 165–180. [[CrossRef](#)]
43. He, F.; Huang, Z.; Law, A. An experimental study of a floating breakwater with asymmetric pneumatic chambers for wave energy extraction. *Appl. Ener.* **2013**, *106*, 222–231. [[CrossRef](#)]
44. Tran, N.; Hung, L.; Kim, S. Evaluation of horizontal and moment bearing capacities of tripod bucket foundations in sand. *Ocean Eng.* **2017**, *140*, 209–221. [[CrossRef](#)]
45. Kim, S.; Hung, L.; Oh, M. Group effect on bearing capacities of tripod bucket foundations in undrained clay. *Ocean Eng.* **2014**, *79*, 1–9. [[CrossRef](#)]
46. *JTS/T 231-2021; Modelling Test for Port and Waterway Engineering*. China Communications Press: Beijing, China, 2021.
47. Ibinabo, I.; Tamunodukobipi, D. Determination of the response amplitude operator(s) of an FPSO. *Engineering* **2019**, *9*, 11. [[CrossRef](#)]

Disclaimer/Publisher’s Note: The statements, opinions and data contained in all publications are solely those of the individual author(s) and contributor(s) and not of MDPI and/or the editor(s). MDPI and/or the editor(s) disclaim responsibility for any injury to people or property resulting from any ideas, methods, instructions or products referred to in the content.